Magneto-elastic coupled finite element analyses

René Billardon — Laurent Hirsinger — Florence Ossart

Laboratoire de Mécanique et Technologie
(E.N.S. de Cachan / C.N.R.S. / Université Paris 6)
61, avenue du Président Wilson, F-94235 Cachan cedex
Florence.Ossart@lmt.ens-cachan.fr

ABSTRACT. *The aim of this paper is to introduce a general framework to model the coupled phenomena which occur when a system of solids is subjected to thermal, magnetic and mechanical loadings. This framework constitutes the basis of the numerical methods to be developed in order to perform coupled thermo-magneto-mechanical structural analyses of electrical machines. These general concepts are illustrated by different examples.*

RÉSUMÉ. *Cet article présente un cadre général pour modéliser les phénomènes couplés qui se produisent quand un système de solides est soumis à des chargements thermiques, magnétiques et mécaniques. Ce cadre donne les bases des méthodes numériques qu'il faut mettre en œuvre pour réaliser l'analyse thermo-magnéto-mécanique couplée des machines électriques. Ces concepts généraux sont illustrés par différents exemples.*

KEY WORDS: *magneto-elastic coupling, magnetic hysteresis, electromagnetic losses, magnetostriction*

MOTS-CLÉS : *couplage magnéto-élastique, hystérésis magnétique, pertes électromagnétiques, magnétostriction.*

Revue européenne des éléments finis. Volume 8 – n° 5-6/1999, pages 525 à 551

1. Introduction

Numerical simulation plays an ever increasing role in the process of advanced electromechanical design and optimisation of electrical machines. Recent progress in this field allows us to contemplate using numerical tools to tackle engineering problems such as the reduction of electromagnetic losses, the reduction of noise emitted by these machines or the development of new micro-actuators. For instance, finite element programs, based on the concepts introduced in this paper, enable us to quantify the influence of assembling and in-service elastic strains on the magnetic behaviour of electromechanical devices.

An accurate treatment of such problems requires a sophisticated modelling of the complex couplings between the different phenomena involved in the real thermo-magneto-mechanical behaviour of electrical machines. Section 2 of this paper presents the two different types of couplings: the global couplings involve the structural conservation laws, whereas the local couplings involve the material behaviour. This paper focuses on this latest type of coupling and Section 3 introduces a general framework to model the local magneto-elastic coupling in the quasi-static case. An internal variable magnetic hysteresis model accounting for stress effect is proposed. This scalar model has been implemented in a 2D finite element program in order to perform electromagnetic structural analyses. Section 4 presents this numerical implementation in detail and also some results which show the effect of the structural eddy currents on the dynamic behaviour of an electrical lamination. Finally, Section 5 presents a simplified analysis of the effect of assembling stresses on the global magnetic behaviour of an electrical machine stator.

2. Thermo-magneto-elastic couplings

Different classes of thermo-magneto-mechanical couplings can be exhibited in magnetic materials: effects of magnetism on mechanics, converse effects of mechanics on magnetism, or any coupling effects between heat transfer and mechanics or magnetism. In order to clarify how these phenomena may be taken into account when developing structural analysis tools, it is proposed herein to classify couplings in terms of global couplings when they correspond to mechanisms at the structural scale, or local couplings when they correspond to the continuum scale.

2.1. *Global (structural) couplings*

So-called global, or structural, couplings involve the conservation laws. For magneto-statics and thermo-elastic cases these conservation laws are the following classical Maxwell, heat transfer and mechanical equilibrium equations:

$$\operatorname{div} \mathbf{B} = 0 \qquad \mathbf{curl\ H} = \mathbf{J} \qquad [1.a] \ \& \ [1.b]$$

$$\operatorname{div} \mathbf{q} + r = 0 \qquad [2]$$

$$\mathbf{div}\ \boldsymbol{\sigma} + \mathbf{f_v} = \mathbf{0} \qquad \varepsilon_{ijk}\,\sigma_{jk} + c_{vi} = 0 \qquad [3.a] \ \& \ [3.b]$$

B, **H**, **J**, **q**, r, $\mathbf{f_v}$, $\mathbf{c_v}$ and $\boldsymbol{\sigma}$ respectively denote the magnetic induction, magnetic field, electrical current density, heat flux, body heat sources, body forces, body couples, and Cauchy stress tensor. Coupled thermo-magneto-mechanical structural analyses consist in seeking the solution to boundary value problems constituted by the set of these conservation laws together with the corresponding boundary conditions and local constitutive equations. In this paper, small displacement and small strain assumptions are made and, consequently, the materials are supposed to remain linear elastic.

A first type of global coupling corresponds to changes in the geometry or in the boundary conditions.

For instance, in an electrical motor the modifications of the magnetic induction map are not only due to the relative rotation of the stator and rotor but also to the variations of the air gap induced by the global deformation of the machine structure. In other words, the geometry and the boundary conditions to be taken into account when solving Maxwell equations should be altered according to the results of the mechanical analysis.

Conversely, an example of the effect of magnetism on mechanics corresponds to the efforts of magnetic origin, i.e. to the surface forces of magnetic origin which should be taken into account through boundary conditions when solving the mechanical equilibrium equations. It is worth noticing that different expressions of these forces of magnetic origin can be found in the literature.

A second type of global coupling corresponds to source terms in the equilibrium equations viz. **j**, r, $\mathbf{f_v}$ and $\mathbf{c_v}$.

For instance, the body forces as well as the body couples of magnetic origin constitute obvious additional source terms in the mechanical problem. As for surface forces of magnetic origin, different incompatible expressions of the body forces of magnetic origin can be found in the literature [MAU 88], [ERI 90].

Another typical example of global coupling corresponds to the fact that the source term r in heat equation [2] includes various terms due to mechanics and electromagnetics as soon as dissipative phenomena are present.

2.2. *Local (material) couplings*

So-called local, or material, couplings involve the material behaviour. They result from the complex interdependence between mechanical, thermal and magnetic phenomena at the atomic scale.

For example, the magnetic anisotropy, and hence the permeability and the coercivity of ferromagnetic materials are affected by temperature and stresses. Conversely, changes in the direction of magnetisation generate so-called magnetostrictive strains. Magnetostriction can be used to build actuators, but it also has negative consequences in many devices (vibrations in electrical machines, internal stresses in magnetic thin film).

Local couplings can be accounted for through an accurate modelling of the complex non-linear behaviour of materials. The development of realistic constitutive equations requires a clear insight of the different microscopic mechanisms responsible for the macroscopic behaviour of the materials. The interactions between these mechanisms should also to be analysed in detail.

This paper is devoted to local couplings between mechanics and magnetism and, more especially, to the effect of elasticity on the magnetic behaviour of soft ferromagnetic materials. A possible approach to develop macroscopic constitutive equations consists in using so-called homogenisation techniques to derive the macroscopic behaviour from microscopic models. Such a multiscale approach has been applied to magneto-mechanics in [BUI 98]. More phenomenological models have been proposed in the literature to couple magnetic and magnetostriction hystereses as well as the stress effect on both types of hysteresis [JIL 95] [SAB 95].

The approach used herein is also phenomenological though based on continuum thermodynamics. This formalism has been considerably extended to develop complex models coupling elasticity, plasticity, phase changes and temperature [LEM 90]. It constitutes a powerful tool, which is used in the following to develop coupled thermo-magneto-elastic constitutive equations.

3. Magneto-elastic modelling and continuum thermodynamics :

3.1. *Some experimental results and their phenomenological interpretation*

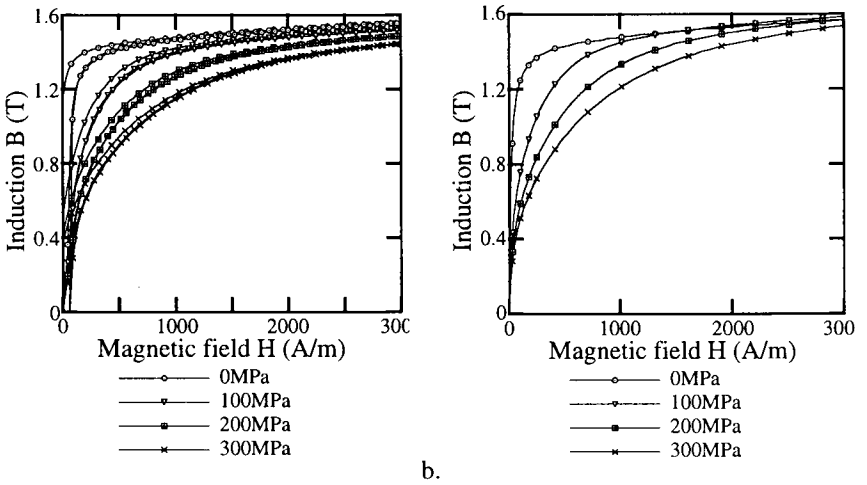

Figure 1. *Effect of elastic tensile stresses on the magnetic behaviour of a Fe-3%Si N.O alloy (M330/50HA) – a. hysteresis loop – b. anhysteretic curve*

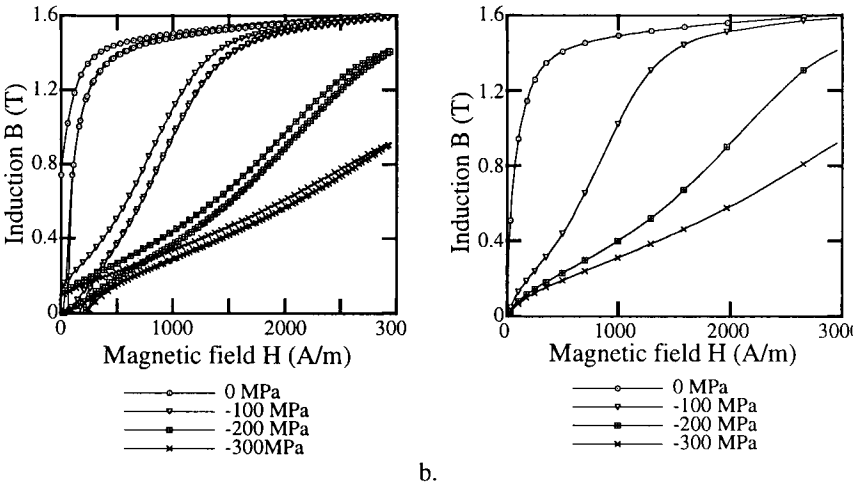

Figure 2. *Effect of elastic compressive stresses on the magnetic behaviour of a Fe-3%Si N.O. alloy (M330/50HA) – a. hysteresis loop – b. anhysteretic curve.*

The experimental results presented in Fig.1 and Fig.2 show the influence of stresses on the magnetic behaviour of an industrial Non-Oriented Fe-3%Si alloy commonly used in electrical power engineering. This material is typically processed

as 0.5 mm thick laminations, which are punched and stacked to build the magnetic circuit of motors. The use of thin sheets is necessary in order to prevent eddy currents which would exist in a bulk material.

Two kinds of measurements are presented: the static hysteresis loops are obtained by cycling the magnetic field between –3000 A/m and +3000 A/m at low frequency (1 Hz in the present case); the anhysteretic curves are measured by superimposing stet the applied field a slowly decaying alternative field in order to reach the state of lowest internal energy. These magnetic behaviours were obtained for uniaxial and colinear mechanic and magnetic excitations applied in the rolling direction of the lamination. The effect of both tensile and compressive stresses was investigated.

These results show that, for the considered material, both uniaxial compressive and tensile elastic stresses alter the magnetic behaviour: a higher magnetic field is required to magnetise the material, and hysteresis losses increase when the material is mechanically loaded. This effect is more important for compressive stresses than for tensile stresses.

3.2. *Phenomenology*

The magnetisation process can be sketched as follows. The material comprises numerous microscopic magnetic domains. In each domain, the magnetisation is uniform (effect of so-called exchange energy) and oriented according to the local orientation of the cristal axes (effect of magnetocrystalline anisotropy energy). The domains are separated by thin walls in which the magnetisation rapidly rotates. At the macroscopic level, if no external field is applied, the average magnetisation tends to be zero because of demagnetising effects.

When an external field is applied, the domain configuration evolves through the domain walls motions: domains oriented in the direction of the external field grow, wheras domains oriented opposite to this direction shrink, so that the average magnetisation changes. During this process, the domain walls motions are withheld by all kinds of defects in the material (impureties, grain boundaries, inclusions, local stresses, etc). Therefore, the magnetic behaviour (magnetisation vs applied field) is hysteretic.

The anhysteretic behaviour corresponds to the behaviour which would be observed for a material with no defect. This ideal behaviour, which corresponds to the state of minimum energy, can be experimentally measured by superimposing stet the applied field a slowly decaying alternative field. This alternating field "shakes" the domain walls and brings the additional energy required to overcome the local energy barriers created by the various obstacles.

Subjecting the material to stresses changes its anisotropy, and hence the magnetic domain configuration and the macroscopic behaviour. The results presented in Fig.1

and Fig.2 show that tensile stresses mainly affect the anhysteretic curve and that in a first approximation, the effect of stresses on the pinning/unpinning of domain walls can be neglected. The case of compressive stresses is more complex, with a change in the shape of the anhysteretic curve and a typical bulging of the hysteresis loop around the demagnetised state.

3.3. *Magneto-elastic continuum thermodynamics [MAU 91] [BAR 95] [GOU 98bis]*

3.3.1. *State variables*

To model the mechanisms described in the previous section, it is proposed to make a partition of the magnetic field into three contributions [4]. For a given applied field, the magnetisation is assumed to be given by the anhysteretic behaviour of the material subjected to an "effective" field $\mathbf{H}_{an}$ laging behind the applied field $\mathbf{H}$ because of hysteresis [5]. This delay is modeled by an internal yielding field $\mathbf{H}_i$ so that the so-called anhysteretic field $\mathbf{H}_{an}$ is defined as sketched on Fig.3.

$$\mathbf{H}_{an} = \mathbf{H} - \mathbf{H}_i \qquad \mathbf{H}_i = \mathbf{H}_{rev} + \mathbf{H}_{irr} \qquad [4]$$

$$\mathbf{M}(\mathbf{H}) = \mathbf{M}_{an}(\mathbf{H}_{an}) = \mathbf{M}_{an}(\mathbf{H} - \mathbf{H}_i) \qquad [5]$$

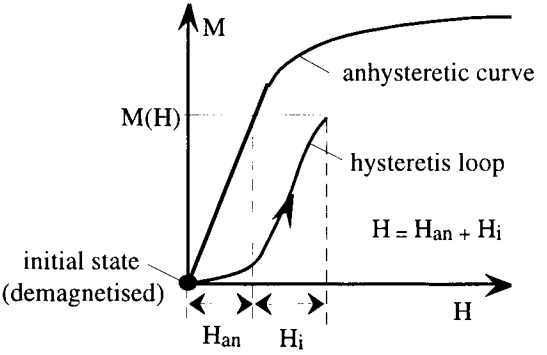

Figure 3. *Definition of the state variables*

The internal field $\mathbf{H}_i$ accounts for the pinning of walls to various obstacles in the material. More detailed mechanisms of the domain wall motions may be modeled by further partitioning the internal field. The reversible bending of the pinned walls may be described by a reversible field $\mathbf{H}_r$ and their irreversible jump to the next obstacle may be described by an irreversible field $\mathbf{H}_{irr}$.

The magnetic field is also responsible for the magnetostriction deformation mechanism. It may be assumed that total strains $\boldsymbol{\varepsilon}$ are the sum of pure mechanical strains $\boldsymbol{\varepsilon}^m$, pure magnetostriction strains $\boldsymbol{\varepsilon}^\mu$ and thermal expansion strains $\boldsymbol{\varepsilon}^{th}$ so that when small strain and linear elasticity assumptions are made, [HIR 96]:

$$\boldsymbol{\varepsilon} = \boldsymbol{\varepsilon}^{m} + \boldsymbol{\varepsilon}^{\mu} + \boldsymbol{\varepsilon}^{th} = \mathbb{E}_{(T)}^{-1} : \boldsymbol{\sigma} + \boldsymbol{\varepsilon}^{\mu}(\boldsymbol{\sigma}, \mathbf{H}, \mathbf{H}_{rev}, \mathbf{H}_{irr}, T) + \boldsymbol{\varepsilon}^{th}(T) \quad [6]$$

where $\mathbb{E}$, $\boldsymbol{\sigma}$ and T respectively denote the elasticity moduli tensor, the stress tensor and temperature. This relation is based on the following uncoupling hypotheses: the elasticity moduli tensor and the thermal dilatation coefficient are supposed not to be affected by the magnetic field.

3.3.2 *State potential*

The specific free enthalpy Ψ may be used as a state potential. It is expressed in [7] as a function of the following state variables: temperature T, stress tensor $\boldsymbol{\sigma}$, magnetic field H and the previously defined internal variables $\mathbf{H}_{rev}$ and $\mathbf{H}_{irr}$. In this formula, ρ denotes the mass density.

$$\rho\Psi = \rho\Psi(\boldsymbol{\sigma}, \mathbf{H}, \mathbf{H}_{rev}, \mathbf{H}_{irr}, T) \quad [7]$$

This global state potential is divided into several uncoupled contributions, each one corresponding to a particular mechanism of the magneto-mechanical behaviour of the material. Formula [8] gives the chosen partition.

$$\rho\Psi = \rho\Psi^{\mu m}(\boldsymbol{\sigma}, \mathbf{H}, \mathbf{H}_{rev}, \mathbf{H}_{irr}, T) + \rho\Psi^{\mu an}(\mathbf{H}-\mathbf{H}_{rev}-\mathbf{H}_{irr}, T) + \rho\Psi^{\mu i}(\mathbf{H}, \mathbf{H}_{rev}, \mathbf{H}_{irr}, T) \quad [8]$$

The first term $\Psi^{\mu m}$ represents the state coupling via the magnetostriction strain. Its expression is postulated as:

$$\rho\Psi^{\mu m}(\boldsymbol{\sigma}, \mathbf{H}, \mathbf{H}_{rev}, \mathbf{H}_{irr}, T) =$$
$$\frac{1}{2}\boldsymbol{\sigma} : \mathbb{E}_{(T)}^{-1} : \boldsymbol{\sigma} + \int_{\mathbf{0}}^{\boldsymbol{\sigma}} \boldsymbol{\varepsilon}^{\mu}\left(\boldsymbol{\sigma}, \mathbf{H}, \mathbf{H}_{rev}, \mathbf{H}_{irr}, T\right) : d\,\boldsymbol{\sigma} + \boldsymbol{\varepsilon}^{th}(T) : \boldsymbol{\sigma} \quad [9]$$

The second term $\rho\Psi^{\mu an}$ is linked to the anhysteretic behaviour of the material. Its expression is postulated in [10], where subscript 0 refers to $\boldsymbol{\sigma}=\mathbf{0}$ and μ_0 denotes the vacuum permeability.

$$\rho\Psi^{\mu an}(\mathbf{H}- \mathbf{H}_{rev}- \mathbf{H}_{irr}, T) = \int_{\mathbf{0}}^{\mathbf{H}-\mathbf{H}_{irr}-\mathbf{H}_{rev}} \mu_0 \mathbf{M}_{an0}(\mathbf{h}, T)\mathbf{dh} \quad [10]$$

The last term $\rho\Psi^{\mu i}$ accounts for the domain wall pinning; it includes reversible mechanisms (domain wall bending) and irreversible ones (unpinning of domain walls).

3.3.3 *State laws and associated thermodynamical forces*

The mechanical and magnetic state laws are derived from the state potential.

$$s = -\frac{\partial \Psi}{\partial T} \qquad [11]$$

$$\boldsymbol{\varepsilon} = \frac{\partial(\rho\Psi^{\mu m})}{\partial \boldsymbol{\sigma}} = \mathbb{B}_{(T)}^{-1} : \boldsymbol{\sigma} + \boldsymbol{\varepsilon}^{\mu}(\boldsymbol{\sigma}, \mathbf{H}, \mathbf{H}_{rev}, \mathbf{H}_{irr}, T) + \boldsymbol{\varepsilon}^{th}(T) \qquad [12]$$

$$\mu_0 \mathbf{M}_1 = \frac{\partial(\rho\Psi^{\mu an} + \rho\Psi^{\mu i})}{\partial \mathbf{H}} + \int_0^{\sigma} \frac{\partial\, \boldsymbol{\varepsilon}^{\mu}}{\partial \mathbf{H}} (\boldsymbol{\sigma}, \mathbf{H}, \mathbf{H}_{rev}, \mathbf{H}_{irr}, T) : d\boldsymbol{\sigma}$$

$$= \mu_0 \mathbf{M}_{an0}(\mathbf{H} - \mathbf{H}_{rev} - \mathbf{H}_{irr}, T) + \int_0^{\sigma} \frac{\partial \boldsymbol{\varepsilon}^{\mu}}{\partial \mathbf{H}} (\boldsymbol{\sigma}, \mathbf{H}, \mathbf{H}_{rev}, \mathbf{H}_{irr}) : d\boldsymbol{\sigma} \qquad [13]$$

$$\mu_0 \mathbf{M}_{rev} = \frac{\partial(\rho\Psi)}{\partial \mathbf{H}_{rev}} \qquad [14]$$

$$\mu_0 \mathbf{M}_{irr} = \frac{\partial(\rho\Psi)}{\partial \mathbf{H}_{irr}} \qquad [15]$$

where s, $\mathbf{M}_1$, $\mathbf{M}_{rev}$ and $\mathbf{M}_{irr}$ respectively denote the entropy and the variables associated to $\mathbf{H}$, $\mathbf{H}_{rev}$ and $\mathbf{H}_{irr}$. The mechanical state law [12] corresponds to equation [6].

The dissipative mechanisms responsible for magnetic hysteresis are linked to the irreversible part $\mathbf{H}_i$ of the magnetic field, and the Clausius Duhem inequality is:

$$D = -\boldsymbol{\varepsilon} : \dot{\boldsymbol{\sigma}} - \mu_0 \mathbf{M} \cdot \dot{\mathbf{H}} + \rho(\dot{\Psi} - s\dot{T}) = \mu_0 \mathbf{M}_{irr} \cdot \dot{\mathbf{H}}_{irr} - \frac{\mathbf{q}.\mathbf{grad}T}{T^2} \quad 0 \qquad [16]$$

3.4. *A scalar magnetic hysteresis model coupled with uniaxial elasticity*

The evolution laws of the internal variables $\mathbf{H}_r$ and $\mathbf{H}_{irr}$ must be chosen such that inequality [16] is satisfied. In [GOU 98bis], a scalar model which accounts for the effect of tensile elastic stresses is proposed. This model is written using the internal field Hi, which includes reversible and irreversible mechanisms in its evolution law. The evolution laws and the zero-stress anhysteretic curve M_{an0} are given by:

$$\dot{H}_i = \chi_0 \dot{H} \qquad \text{if } \dot{H} > 0 \text{ and } H_i \; H_y$$

$$\text{or if } \dot{H} < 0 \text{ and } -H_y \; H_i \qquad [17.a]$$

$$\dot{H}_i = f(H, H_i)\dot{H} = \frac{H_c - \delta H_i}{H_c - H_y} \chi_0 \dot{H} \qquad \text{with } \delta = \mathrm{sgn}(\dot{H}) \qquad \text{else} \qquad [17.b]$$

$$M_{an0}(H - H_i) = \frac{2 M_s}{} \text{Arctan}\left(\frac{\pi}{2} \chi_{a0} \frac{H - H_i}{M_s}\right) \qquad [18]$$

where constants χ_0, χ_{a0}, M_s, H_c and H_y denote material parameters respectively related to the initial slopes of the magnetisation and anhysteretic curves, the saturation magnetisation, the coercive magnetic field and a so-called yield magnetic field.

For the sake of simplicity, the coupling between magnetic hysteresis and elasticity is assumed to affect only the anhysteretic curve through stress dependent parameters. In the considered range of tensile stress and for the studied material, a linear relationship between the initial slope of the anhysteretic curve and stress is found to represent well the stress dependence of the magnetic behaviour. For a given stress σ, the anhysteretic curves M_{an} are given by the following expression:

$$M_{an}(H - H_i, \sigma) = \frac{2 M_s}{} \text{Arctan} \left(\frac{\pi}{2} \chi_a(\sigma) \frac{H - H_i}{M_s} \right) \quad [19]$$

$$\text{with} \quad \chi_a(\sigma) = \chi_{a0} + A \,.\, \sigma \quad [20]$$

where χ_{a0} and A correspond respectively to the value of the uniaxial stress applied in the direction of the magnetic field and a constant.

These simple assumptions give a good approximation of the B(H) loops for different tensile stresses, as shown Figure 4.

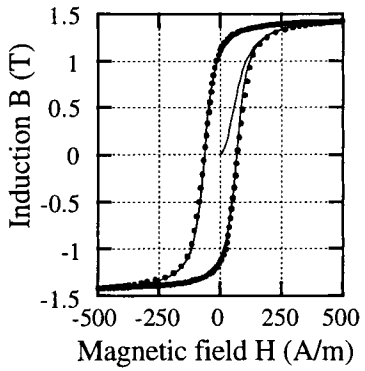

a. $\sigma = 0$ Mpa

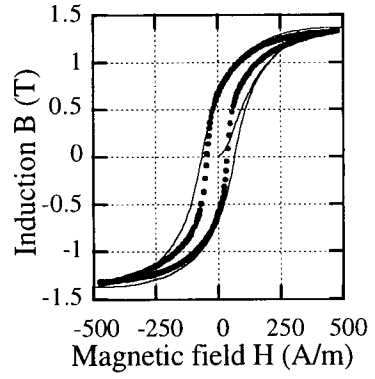

b. σ = 50 Mpa

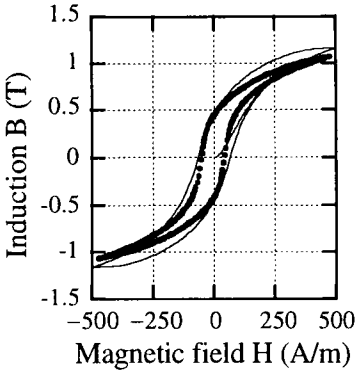

c. σ = 150 Mpa

Figure 4. *Hysteresis loops of a Fe-3%Si N.O. alloy (M330/50HA) for various tensile stresses, comparison between experiments (points) and model (solid line)*
– *a.* $\sigma = 0$ *Mpa – b.* $\sigma = 50$ *Mpa – c.* $\sigma = 150$ *Mpa.*

4. Implementation of the internal variables magnetic hysteresis model in a finite element fully coupled analysis

The model presented in the previous section takes into account the influence of elastic stresses on the local magnetic properties and it must be noticed that a local change of the magnetic properties affects the magnetic field distribution at the scale of the structure. To investigate this global influence of stresses, it is necessary to implement the coupled hysteresis model in a finite element code. A weak magneto-elastic coupling, valid in many usual cases, can be assumed. The stress distribution is the result of a previous calculus, either analytical or numerical, and the stress induced by magnetostriction is neglected. The resulting local magnetic properties

are predicted by the hysteresis model and the magnetic field distribution is computed by solving Maxwell's equations.

At the present stage of our work, we have implemented the internal variable magnetic hysteresis model without effect of the local stress in a 2D magnetodynamic finite element computation. This numerical tool has been used to predict the influence of eddy currents on the dynamic behaviour of a magnetic lamination. The magneto-elastic coupled hysteresis model is currently being implemented according to the principles described hereunder, in order to extend the presented results.

4.1. *2D vector potential formulation*

The global magnetic problem consists in solving the low frequency Maxwell equilibrium equations [21] with corresponding boundary conditions and the material constitutive equations [22].

$$\mathbf{curl}\ \mathbf{H} = \mathbf{J}_{tot} \qquad \mathbf{curl}\ \mathbf{E} = -d\mathbf{B}/dt \qquad \mathrm{div}\ \mathbf{B} = 0 \qquad [21]$$

$$\mathbf{B} = \mathbf{B}(\mathbf{H})\ (\text{ or } \mathbf{H} = \mathbf{H}(\mathbf{B})\ ) \qquad \mathbf{J}_{tot} = \sigma\,\mathbf{E} \qquad [22]$$

where $\mathbf{H}$, $\mathbf{B}$, $\mathbf{J}_{tot}$, $\mathbf{E}$ and σ respectively denote the magnetic field, magnetic induction, electric current density, electric field and electrical conductivity.

We consider a 2D problem defined in the (x,y,z) coordinate system by:

$$\mathbf{B} = \begin{bmatrix} B_x(x,y) \\ B_y(x,y) \\ 0 \end{bmatrix} \quad \mathbf{H} = \begin{bmatrix} H_x(x,y) \\ H_y(x,y) \\ 0 \end{bmatrix} \quad \mathbf{J} = \begin{bmatrix} 0 \\ 0 \\ J_z(x,y) \end{bmatrix} \quad \mathbf{E} = \begin{bmatrix} 0 \\ 0 \\ E_z(x,y) \end{bmatrix} \qquad [23]$$

The vector magnetic potential $\mathbf{A}$ and the scalar electric potential V are defined by [24.a] and [24.b], so that $\mathbf{B}$ is always divergence-free.

$$\mathbf{B} = \mathbf{curl}\ \mathbf{A} \qquad \mathbf{E} = -\,d\mathbf{A}/dt - \mathbf{grad}\ V \qquad [24.a]\ \&\ [24.b]$$

For the considered 2D-problem, $\mathbf{A}$ has only one non zero component, according to [25.a] and the electric potential V(x,y) is constant over the (x,y) plane.

$$\mathbf{A} = \begin{bmatrix} 0 \\ 0 \\ A_z(x,y) \end{bmatrix} \qquad V(x,y) = Vo \qquad [25.a]\ \&\ 25.b]$$

The current density $\mathbf{J}_{tot}$ may be divided into two parts: $\mathbf{J}_{tot} = \mathbf{J} + \mathbf{J}_{eddy}$, where $\mathbf{J}$ denotes the current density imposed by the external electrical circuit, and $\mathbf{J}_{eddy}$ denotes the eddy current density due to the electric field induced by the time variations of the induction, so that:

$$\mathbf{J}_{tot} = \mathbf{J} + \sigma\,\mathbf{E} \qquad \text{with} \qquad \mathbf{E} = -\,d\mathbf{A}/dt \qquad [26]$$

The dynamic behaviour is finally given by the set of equations [27].

$$\mathbf{curl H} + \sigma \frac{d\mathbf{A}}{dt} = \mathbf{J} \qquad \text{with } \mathbf{H}=\mathbf{H}(\mathbf{B}) \text{ and } \mathbf{B} = \mathbf{curl\ A} \qquad [27]$$

Three numerical methods are required to numerically solve equation [27] [HIR 96] [BEN 88] : θ-method time stepping scheme for the time discretisation, finite element method for the space discretisation, Newton method to solve the resulting non linear system of equations at each time step.

Let us assume that the problem has been solved at time t_n. The next time step is $t_{n+1} = t_n + \Delta t$. The θ-method assumes a linear time variation of all values during Δt, so that:

$$(\bullet)_{n+\theta} = (1-\theta)\,(\bullet)_n + \theta\,(\bullet)_{n+1}\,, \text{ with } 0 \quad \theta \quad 1. \qquad [28]$$

Combining [27] and [28] leads to:

$$\theta\ \mathbf{curlH}_{n+1} + \frac{\sigma}{\Delta t}\mathbf{A}_{n+1} = \mathbf{J}_{n+\theta} - \left(1-\theta\right)\mathbf{curlH}_n - \frac{\sigma}{\Delta t}\mathbf{A}_n \qquad [29]$$

The variational formulation is obtained by Galerkine method, which leads after some calculus to [30], where $\mathbf{A}^*$ is a suitable test function, satisfying the boundary conditions of the problem [MAR-91].

$$\theta \int_\Omega \mathbf{H}_{n+1}\ \mathbf{curlA}^*\ d\Omega + \frac{\sigma}{\Delta t}\int_\Omega \mathbf{A}_{n+1}\ \mathbf{A}^*\ d\Omega = \int_\Omega \mathbf{J}_{n+\theta}\ \mathbf{A}^*\ d\Omega - \left(1-\theta\right)\int_\Omega \mathbf{H}_n\ \mathbf{curlA}^*\ d\Omega + \frac{\sigma}{\Delta t}\int_\Omega \mathbf{A}_n\ \mathbf{A}^*\ d\Omega \qquad [30]$$

It must be noticed that because of the particular form of vectors A and J, this functional leads to a single scalar equation which is written in terms of Az and Jz respectively denoted A and J in the rest of the paper.

4.2. *Linear case*

The domain is discretized and potential A is given by [31] where Ni denote the interpolation functions.

$$A = \sum_{\text{nodes}} A_i\ N_i \qquad [31]$$

If we assume a linear magnetic behaviour defined by $\mathbf{H} = \nu\ \mathbf{B}$, where ν denotes the magnetic reluctivity, the magnetic field $\mathbf{H}$ is expressed as follows:

$$\mathbf{H} = \nu \sum_{\text{nodes}} A_i\ \mathbf{curl} N_i \qquad [32]$$

We use the interpolation functions as test functions, and the linear system to be solved becomes:

$$\left(\theta\ [S] + [C]\right)\ \{A\}_{n+1} = \{J\}_{n+\theta} + \left(-(1-\theta)\ [S] + [C]\right)\ \{A\}_n \qquad [33]$$

where $\{A\}_n$ denotes the nodal values vector at time t_n, [S] and [C] denote the reluctivity and the electric conductivity matrices and $\{J\}_{n+\theta}$ denotes the source vector at time $t_{n+\theta}$, respectively defined by the general expressions:

$$[S] = [S_{ij}] = \left[\int_\Omega \nu\ \mathbf{curl}^T N_i\, \mathbf{curl} N_j\ d\Omega\right] \qquad [34]$$

$$[C] = [C_{ij}] = \left[\int_\Omega \frac{\sigma}{\Delta t} N_i N_j\ d\Omega\right] \qquad [35]$$

$$\{J\} = \{J_j\} = \left\{\int_\Omega J\ N_j\ d\Omega\right\} \qquad [36]$$

4.3. *General case*

In the general case, the B(H) relationship is not linear and an iterative computation is required to solve the system. At each time step, the Newton method is applied. The residual vector {R(A)} is defined by the general term R_j:

$$\begin{aligned} R_j \quad = \quad & \theta \int_\Omega \mathbf{H}_{n+1}\ \mathbf{curl} N_j\ d\Omega \ + \frac{\sigma}{\Delta t}\int_\Omega A_{n+1}\ N_j\ d\Omega \\ & - \int_\Omega J_{n+\theta}\ N_j\ d\Omega + (1-\theta)\int_\Omega \mathbf{H}_n\ \mathbf{curl} N_j\ d\Omega \ - \frac{\sigma}{\Delta t}\int_\Omega A_n\ N_j\ d\Omega \end{aligned} \qquad [37]$$

At iteration s+1, the new estimation A_{n+1}^{s+1} of the solution is computed by solving [38], where A_{n+1}^{s} denotes the previous estimation.

$$R\left(A_{n+1}^{s+1}\right) = R\left(A_{n+1}^{s}\right) + \left[\frac{dR}{dA}\right]_{n+1}^{s}\left(A_{n+1}^{s+1} - A_{n+1}^{s}\right) = 0 \qquad [38]$$

After some calculus, the system to solve is:

$$\left(\theta\,[\mathrm{Stg}]^{s}_{n+1} + [\mathrm{C}]\right)\left(\{\mathrm{A}\}^{s+1}_{n+1} - \{\mathrm{A}\}^{s}_{n+1}\right) = \{\mathrm{J}\}_{n+\theta} + \left(-(1-\theta)\,[\mathrm{Ssc}]_{n} + [\mathrm{C}]\right)\{\mathrm{A}\}_{n} - \left(\theta\,[\mathrm{Ssc}]^{s}_{n+1} + [\mathrm{C}]\right)\{\mathrm{A}\}^{s}_{n+1} \quad [39]$$

[Stg] and [Ssc] are the tangential and secant reluctivity matrices, defined by:

$$[\mathrm{Stg}] = [\mathrm{Stg}_{ij}] = \left[\int_{\Omega} \mathbf{curl}^{\mathrm{T}}\mathrm{N}_{i}\left[\frac{\mathrm{dH}}{\mathrm{dB}}\right]\mathbf{curl}\mathrm{N}_{j}\;\mathrm{d}\Omega\right] \quad [40]$$

$$[\mathrm{Ssc}] = [\mathrm{Ssc}_{ij}] = \left[\int_{\Omega} \mathbf{curl}^{\mathrm{T}}\mathrm{N}_{i}\left[\frac{\mathrm{H}}{\mathrm{B}}\right]\mathbf{curl}\mathrm{N}_{j}\;\mathrm{d}\Omega\right] \quad [41]$$

Δt is chosen small enough to describe properly the local hysteresis loops at each computation point of the sheet section and to accurately compute field variations and resulting eddy currents. The chosen value of θ is 0.5, which corresponds to the inconditionnally stable Crank-Nicolson algorithm.

4.4. *Numerical implementation of the hysteresis model*

To compute the matrices [Stg] and [Ssc] needed in [39] to determine the field distribution in the device at time t_{n+1}, one needs to know the field H and the differential reluctivity dH/dB for the induction B and the state of the material at time t_n.

At time t_n, the state of the material is defined by the values H_n and Hi_n of the state variables. The behaviour of the material is governed by the non-linear equations [17] and [18], which are numerically solved by a θ-method and Newton algorithm. Variables H, Hi, M and B are linked by evolution law [42], anhysteretic curve [43] and constitutive equations [44]:

$$\dot{\mathrm{H}}_{\mathrm{i}} = \mathrm{f}(\mathrm{H}, \mathrm{H}_{\mathrm{i}})\,\dot{\mathrm{H}} \quad [42]$$

$$\mathrm{M}(\mathrm{H}) = \mathrm{M}_{\mathrm{an}}(\mathrm{H} - \mathrm{Hi}) \quad [43]$$

$$\mathrm{B} = \mu_{0}\,[\mathrm{H} + \mathrm{M}(\mathrm{H})] \quad [44]$$

Evolution law [42] is discretized in the incremental form:

$$\Delta Hi = f(Hi_{n+\theta}, H_{n+\theta})\,\Delta H \qquad \text{where } \Delta Hi = Hi_{n+1} - Hi_n \quad \text{and} \quad \Delta H = H_{n+1} - H_n \qquad [45]$$

Constitutive equation [44] combined with the magnetisation evolution defined in [43] leads to the following relationship between the given induction B_{n+1} and the unknown variables H_{n+1} and Hi_{n+1}.

$$B_{n+1} = \mu_0 \left[H_{n+1} + M_{an}(H_{n+1} - Hi_{n+1}) \right] \qquad [46]$$

The set of equations [45] and [46] is numerically solved using Newton algorithm to determine H_{n+1} and Hi_{n+1}. Special care must be taken because the evolution law [42] has two possible analytical expressions, depending on the current value of Hi (reversible and irreversible cases). It must also be stressed out that the state of the material, defined by H_n and Hi_n, should not be updated before convergence of the Newton algorithm has been reached. The calculated values H^s_{n+1} and Hi^s_{n+1} are only intermediate values which must be discarded.

4.5. *Prediction of the dynamic behaviour of electrical laminations [HIR-98]*

The magnetic constitutive equations presented above have been implemented in the finite element software package CASTEM 2000. This software is mainly dedicated to thermo-mechanical structural analysis, but 2D electromagnetic problems can be handeled by a proper analogy with heat transfer analyses [HIR 94] [HIR 96] [HIR 98].

The electromagnetic finite element model with hysteresis was used to investigate the dynamic behaviour of an electrical lamination. It is known that macroscopic eddy currents developping at high frequency reduce the apparent permeability of conductive materials and increase hysteresis and losses. But it is not always clear if this effect is the only one involved in the dynamic behaviour of the lamination. The local magnetic behaviour M(H) itself may be rate-dependent. To identify if such a local frequency effect exists and if an additional rate effect should be introduced in the local magnetic hysteresis model, it is proposed to proceed as follows.

First, the quasi-static behaviour of the material is measured and used to identify the parameters of the hysteresis model. Then, the dynamic behaviour of the material is measured and calculated with the finite element model for various frequencies. Discrepancies between the measured and modelled dynamic behaviours are attributed to the local frequency effect, which is not accounted for in the finite element model.

This procedure was applied to identify if any frequency effect exists in the case of a 0.5 mm thick industrial non oriented Fe-3%Si magnetic lamination. The virgin magnetisation curves - that is the magnetisation curves obtained for an initially demagnetised state and zero-stress - were used for this study. A 12.5 mm wide and

200 mm long sample of the considered material was subjected to an external field H_s applied in the direction of the sample. The resulting magnetic flux was obtained by measuring the voltage induced in a coil wrapped around the sample. Then, the average induction $B(H_s)$ was plotted as a function of the surface field. Fig.5 shows the principle of the device.

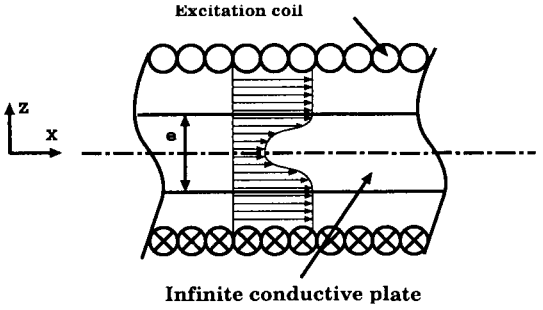

Figure 5. *Infinite conductive plate*

In the quasi-static case, no eddy currents affect the measurement, and the global behaviour is also the local one. The experimental virgin curve was used to determine the parameters of the model and a very good fit could be obtained, as shown in Fig.6. The set of parameters used is: $\chi_0 = 0.975$, $\chi_{a0} = 34650$, $M_s = 1\ 088\ 735$ A/m, $H_c = 70$ A/m and $H_y = 10$ A/m.

Fig.7 shows the effect of frequency on the global behaviour. The virgin magnetisation curve is measured for a magnetic field applied at a rate ranging from 10^4 to $1{,}4.10^6$ A/m/s. As the field rate increases, the material becomes harder to magnetise through its whole thickness because eddy currrents slow down any flux time variation.

The lamination can be modelled as an infinite conductive plate, as shown in Fig.5, because its width is very large compared to the thickness (0.5mm). The global dynamic behaviour of the material is predicted by the finite element model described hereabove which includes hysteresis and the structural eddy currents. The parameters of the model are the ones previously identified, and the electrical conductivity is given by the lamination manufacturer ($\sigma = 2.22\ 10^6\ (\Omega m)^{-1}$). The induction is not uniform in the lamination thickness and its mean value is given by formula [47] where e denotes the thickness of the lamination. The calculated global behaviours are compared to the experimental ones on Fig.7.

$$\overline{B} = \frac{1}{S}\int \mathbf{B}\,.\,\mathbf{dS} = \frac{1}{e}\int_{-e/2}^{e/2} B(y)\,dy = \frac{\phi}{S} \qquad [47]$$

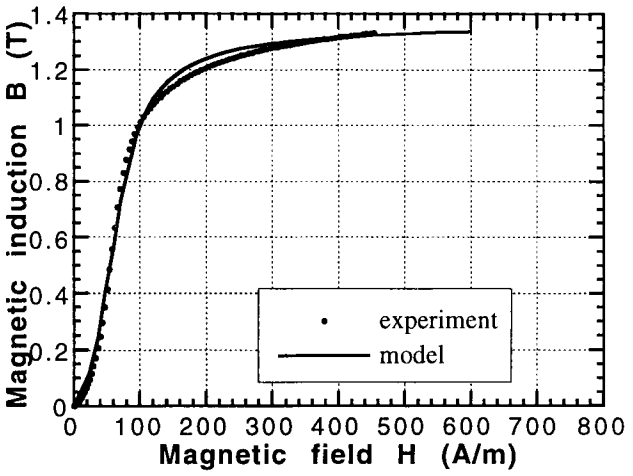

Figure 6. *Quasi-static virgin magnetisation curve of the lamination (Fe-3%Si N.O. 0.5 mm thick)*

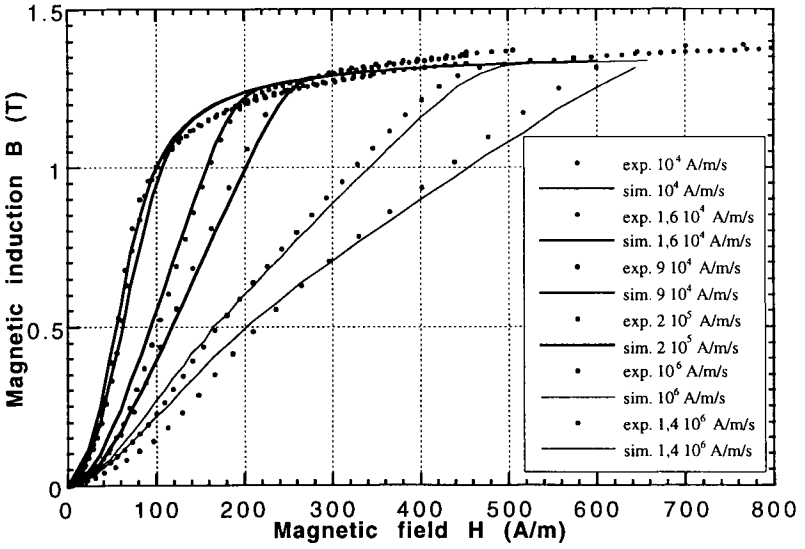

Figure 7. *Frequency dependence of the global virgin magnetisation curve (M330/50HA); comparison between measured and predicted virgin curves.*

It can be concluded that, for the considered material subjected to uniaxial magnetic loading in the rolling direction, no local frequency effect needs to be introduced in the local magnetic hysteresis model. Some authors [ROU 96] [CHE 86] and [JIL 95] have opposite conclusions for other Fe-Si laminations. It is now established that the local frequency effect is very dependent on the grain size of the material. Hence, our conclusion is consistent with studies indicating that a local frequency effect should be expected in materials with large grain size (about 30 μm in our case).

5. Finite element implementation of a magneto-elastic coupled anhysteretic model

We have proposed in Section 3 a simple hysteresis model accounting for the effect of tensile stresses. In the present section, we focus on compressive stresses, which have a stronger and more complex effect than tensile stresses. The anhysteretic curve is very degraded and inflexion points appear, preventing the use of simple analytical functions to model it. Moreover, not just the anhysteretic curve is affected. The coercive field increases and a more complex coupled magneto-elastic model should be built.

In this section we propose to use a simple approach to model the magneto-elastic coupling. Only the anhysteretic curve is used and hysteresis losses are computed by a post-treatment of the stuctural analysis. This coupled model is used to investigate the consequence of the local stress effect at the global scale of a device in the case of a machine stator subjected to assembling stresses. The considered material is a slightly different electrical lamination than the previous one (low silicium iron alloy M1000/65D, thickness = 0.65mm). Experimental and computed results show similar increases of hysteresis losses when assembling stresses are present.

5.1. *Principle of the magneto-elastic coupled finite element model*

Again a weak magneto-elastic coupling, valid in many cases, is assumed: the magnetic field is computed for a given elastic stress distribution, stresses induced by magnetostriction being assumed to be negligible.

For the sake of simplicity only the anhysteretic behaviour of the material is modelled and hysteresis losses are computed by post-treatment of the structural analysis. The analysis is divided into three successive steps:

– Computation of the stress distribution $\sigma(x,y)$ by a 2D elastic finite element model.

– Computation of the magnetic field and induction distributions by a 2D magnetostatic finite element model. The magnetic behaviour of the material is accounted for by a non-linear scalar stress-dependent anhysteretic model $B_{an}(H,\sigma)$,

the stress map being the result of the first step. The vector magnetic potential formulation is applied and a Newton method is used to solve this non-linear system.

– Computation of hysteresis losses using a stress-dependent model $L_{an}(B, \boldsymbol{\sigma})$.

A scalar model $B_{an}(H,\boldsymbol{\sigma})$ is used, which is obtained for unidirectionnal and colinear mechanical and magnetic excitations. Since we are performing a 2D computation, choices are made in order to define the sensible norms of **B**, **H** and $\boldsymbol{\sigma}$ to be used.

We assume plane stress conditions. Hence the resulting stress $\boldsymbol{\sigma}$ is a tensor with two non-zero components in the local principal stresses coordinate system. The equivalent scalar stress we choose as an input of the scalar $B_{an}(H,\sigma)$ model is the largest principal stress, the effect of the other one being neglected. Using Von Mises equivalent stress as norm of $\boldsymbol{\sigma}$ would not account for the non-symmetric effects of tensile and compressive stresses. An isotropic magnetic behaviour is assumed, meaning that H and B are colinear and that their moduli are used in the relationship $B_{an}(H,\sigma)$. Anisotropy induced by stress is not accounted for.

The 2D-problem we are solving is simpler that the one presented in the previous section. Eddy currents are not taken into account and the equations to be solved are:

$$\mathbf{curl}\ \mathbf{H} = \mathbf{J} \qquad \text{div}\ \mathbf{B} = 0 \qquad \mathbf{B}=\mathbf{B}(\mathbf{H}) \qquad [48]$$

With the notations used in Section 4, for a given value of the feeding current density J, the residual vector is:

$$R_j = \int_\Omega \mathbf{H}\ \mathbf{curl}N_j\ d\Omega - \int_\Omega J\ N_j\ d\Omega \qquad [49]$$

This nonlinear equation is solved using Newton technique. At iteration s+1, system [50] is solved, where A_s is the solution resulting from the previous Newton iteration and A_{s+1} is the new estimation of the solution.

$$R\left(A_{n+1}^{s+1}\right) = R\left(A_{n+1}^{s}\right) + \left[\frac{dR}{dA}\right]_{n+1}^{s}\left(A_{n+1}^{s+1} - A_{n+1}^{s}\right) = 0 \qquad [50]$$

After some calculus, the equation to be solved is:

$$[Stg]^s\left(\{A\}^{s+1} - \{A\}^s\right) = \{J\} - [Ssc]^s\ \{A\}^s \qquad [51]$$

[Stg] and [Ssc] are the tangential and secant reluctivity matrices, defined in Section 3 by formula [40] and [41].

5.2. *Effect of compressive stresses*

The stator of the studied machine is subjected to compressive stresses reaching up to 100 MPa. Fig.7 and Fig.9 show the drastic influence of such stresses on the anhysteretic curve and on hysteresis losses measured on a ribbon of the studied alloy. These curves show two effects. First, the anhysteretic curve and the hysteresis loops (not presented here) are tilted, which will affect the field distribution and require a higher feeding current to magnetise the device. The second effect is the increase of hysteresis losses, which increases the global losses.

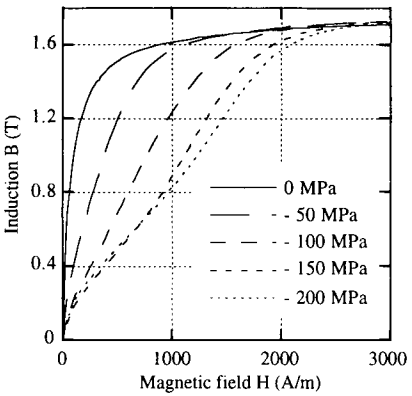

Figure 8. *Influence of compressive elastic stresses on the anhysteretic curve (M1000/65D grade)*

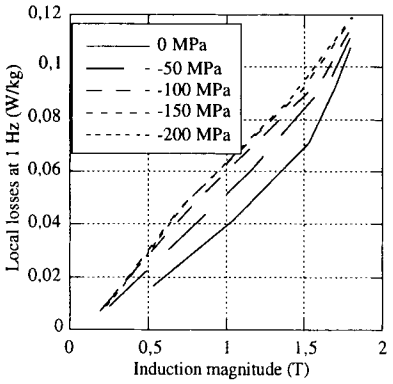

Figure 9. *Influence of compressive elastic stresses on hysteresis losses (M1000/65D grade)*

The anhysteretic behaviour $B_{an}(H,\sigma)$ needed in the finite element model is reproduced by a two-step interpolation of the set of curves of Fig.8. First, each measured curve is modelled using Akima's interpolation [AKI-70]. This method of interpolation is a semi-spline method based on a local procedure, which prevents the unnatural oscillations of classical spline methods. Then, the $B_{an}(H,\sigma)$ curve corresponding to a stress value σ between σ_1 and σ_2 is built using a linear interpolation of curves $B_{an}(H,\sigma_1)$ and $B_{an}(H,\sigma_2)$. For a given value of the induction B, H_σ is computed by formula [52], $H_{\sigma 1}$ and $H_{\sigma 2}$ being defined on Fig.10.

$$H_\sigma = \alpha H_{\sigma 1} + \beta H_{\sigma 2} \quad \text{with } \beta = \frac{\sigma - \sigma 1}{\sigma 2 - \sigma 1} \quad \text{and } \alpha = 1 - \beta \qquad [52]$$

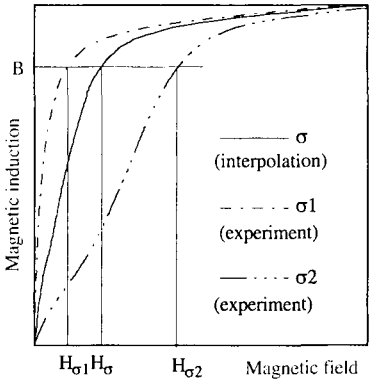

Figure 10. *Principles of the interpolation of the anhysteretic curve*

Modelling losses turns out to be very simple if one plots the losses as a function of the $B_{max}.H_{max}$ product, where B_{max} and H_{max} respectively denote the induction and field magnitude of the hysteresis loop. This function does not depend on the applied stress and can be fitted by analytical formula [53]. Fig.11 shows the very good result obtained with $\alpha = 5.25.10^{-2}$, $\beta = 1034$, $\gamma = 1.07.10^{-3}$ and $\delta = 0.459$.

$$L_{hys}(H_{max}.B_{max}) = \alpha\left[1 - \exp\left(-\frac{H_{max}.B_{max}}{\beta}\right)\right] + \gamma(H_{max}.B_{max})^{\delta} \qquad [53]$$

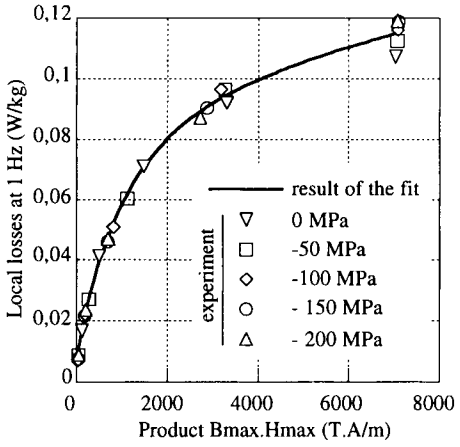

Figure 11. *Evolution of hysteresis losses vs Hmax.Bmax product*

5.3. *Influence of compressive assembling stresses on the global magnetic behaviour of an electrical machine stator [OSS 99]*

In order to demonstrate the influence of elastic stresses at the global scale of an industrial device, measured and calculated hysteresis losses in an electrical machine stator are compared in the case where the stator is subjected to assembling stresses and in the case where no mechanical loading is present. A simple test device (Fig.13) is derived from an industrial motor by hooping the magnetic circuit of the stator in an aluminium ring similar to the motor-housing. Feeding and pick-up coils are wound all around the structure, in order to measure the global magnetic behaviour of the structure.

The stator is subjected to non uniform compressive stresses, with a sharp increase of magnitude at the root of the slots. The radial stress which is neglected in our model, reaches 15% of the circonferential stress. Stresses are proportional to the contact pressure p_c which in turn is proportional to the difference of radius δ between the stator and the ring. Two devices, corresponding respectively to $p_c = 2.3$ MPa and $p_c = 6.2$ MPa, have been studied.

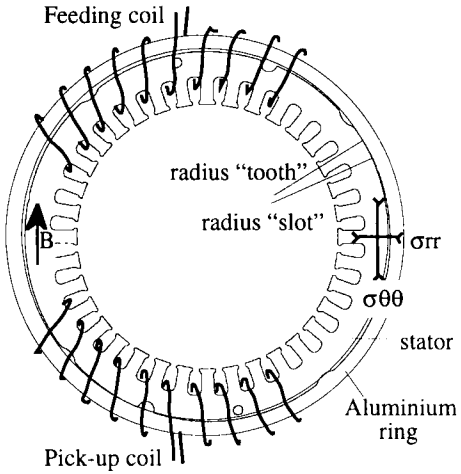

Figure 12. *Principle of the studied device.*

First the global behaviour of the devices (flux in the stator vs feeding current, losses vs flux) is measured, then the ring is cut in order to remove assembling stresses and the magnetic behaviour is measured again. The effect of stresses, if any, is then clearly pointed out. The corresponding simulations are performed by using CASTEM 2000. The computed results are compared to the experimental data on Fig.13 and Fig.14. For an easier interpretation of the results, the flux is expressed as the average induction in the stator.

Experimental results show, as expected, that because of assembling stresses a higher feeding current is required to magnetise the stator and that losses do increase. For an average induction of 0.5 T, the relative increase of losses is about 30% for p_c = 2.3 MPa and 60 % for p_c = 6.2 MPa. This drastic increase of losses in the stator should be weighted by their relative contribution to the total losses of the motor.

The finite element model gives trends very similar to the experimental ones, but the computed behaviour is too optimistic. This can be explained in part by the fact that the material anisotropy is neglected and that only the behaviour in the rolling direction is used, although the magnetic properties in other directions are significantly degraded. Furthermore it is recalled that the stress state in the stator is biaxial whereas the simple scalar model used herein takes account of a scalar stress equal to the largest principal stress. The finite element simulation also shows that for a given flux in the stator the stress non uniformity alters much more the field than the induction distribution.

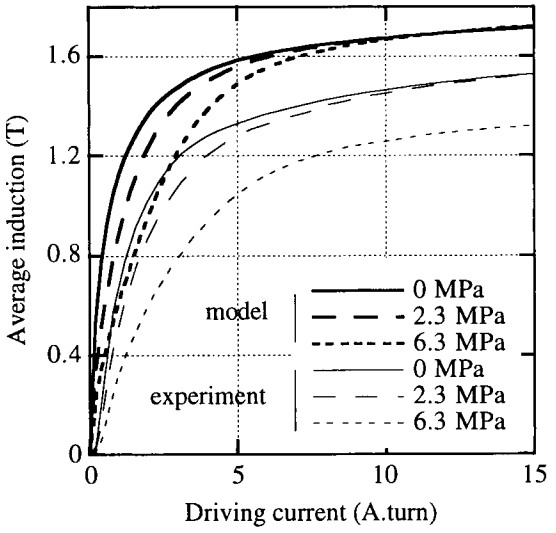

Figure 13. *Global behaviour of the stator (average induction vs feeding current)*

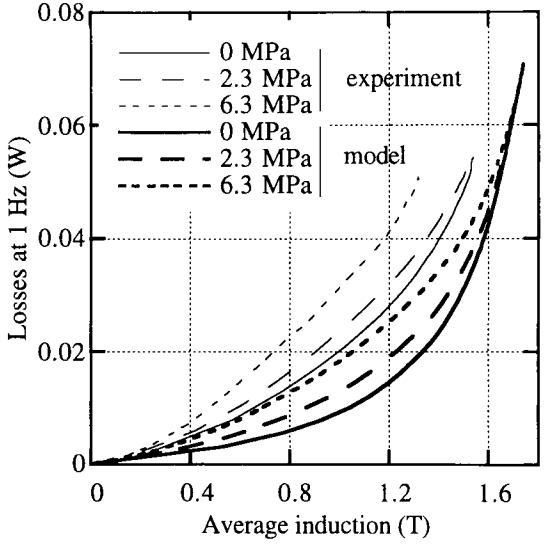

Figure 14. *Hysteresis losses vs average induction in the stator*

6. Conclusions

A general framework has been proposed in order to model electro-magneto-mechanical couplings. Two constitutive models have been proposed in order to account for the influence of stresses on the magnetic behaviour of ferromagnetic materials, each one corresponding to a different simplification of the complex real phenomena. The present scalar version of the internal variable hysteresis model is suitable to describe tensile stress effect and can be applied only for uniaxial magnetic loadings. The isotropic anhysteretic magnetic model accounts for compressive stresses and can be used for 2D magnetic loading. These models have been implemented in finite element structural analyses in order to model practical examples where only some magneto-elastic couplings play a key role.

In some cases, phenomena such as thermo–electro-magneto-mechanical couplings may play a prominent role. The formal introduction of these couplings in the general framework above-described is rather straightforward [MAU 88] [ERI 90], and many examples of coupled electro-magnetic or electro-mechanical numerical analyses may be found in the recent literature.

As a conclusion, it is worth noticing that in such coupled analyses, most open problem are not related to the numerical formulations but to the modelling of the complex local behaviour of the materials. The development of the corresponding realistic highly nonlinear coupled local constitutive equations cannot be contemplated as a simple extension of the presently available models and many efforts are still needed in this area.

Acknowledgements

Part of this work has been carried out in collaboration with Eric HUG from LGMMS of Compiègne (France) and supported by GIRTOM (Groupement des Industriels et Centres de Recherche dans le domaine des Tôles Magnétiques, France).

References

[AKI 70] AKIMA H., J. ACM, **17** (1970), 589.

[BAR 95] BARBIER G., « Proposition d'un modèle de couplage magnéto-mécanique pour les matériaux ferromagnétiques doux », Rapport du DEA de Mécanique, Université Paris VI, LMT Cachan, 1995.

[BEN 88] BENALLAL A., BILLARDON R, DOGHRI I., "An integration algorithm and the corresponding consistent tangent operator for fully coupled elastoplastic and damage equations", *Communications in Applied Numerical Methods*, 4 (1988) 731-740.

[BUI 98] BUIRON N., HIRSINGER L.,BILLARDON R., "A multiscale model for magneto-elastic couplings", *J. Phys.* IV France 9, (1999), Pr9-187-196.

[CHE 86] CHEN C.-W., "Magnetism and metallurgy of soft magnetic materials", Dover Publication, New York, 1986.

[ERI 90] ERINGEN A.C. & MAUGIN G.A., *Electrodynamics of continua*, Springer Verlag, 1990.

[GOU 98] GOURDIN C., HIRSINGER L., BARBIER G. et BILLARDON R., "Experimental identification of the coupling between the anhysteretic magnetic and magnetostrictive behaviours", J. Magn. Mag. Mat., 177-181 (1998) 201-202.

[GOU 98bis] GOURDIN C., Identification et modélisation du comportement électromagnétique de structures ferromagnétiques, Thèse de Doctorat, Université Paris VI, LMT-Cachan, Janvier 1998.

[HIR 94] HIRSINGER L., Etude des déformations magnéto-élastiques dans les matériaux ferromagnétiques doux, Thèse de doctorat de l'Université Paris VI, décembre 1994.

[HIR 96] HIRSINGER L., BILLARDON R., "Static and dynamic 2-D magnetic analysis with an internal variables hysteresis model", *Numerical Methods in Engineering'96*, 2nd ECCOMAS Proc., Wiley, 1996, p. 318-324.

[HIR 98] HIRSINGER L., GOURDIN C., BILLARDON R., "Identification of the frequency effect on magnetic hysteresis and modelling with an internal variables model", *J. Phys. IV* France 8, (1998), Pr2-655-658.

[JIL 95] JILES D.C., "Theory of the magnetomechanical effect", *J. Phys.* D: Applied Physics, 28 (1995), 1537-1546.

[LEM 90] LEMAITRE J. & CHABOCHE J.-L., *Mechanics of solid materials*, Cambridge University Press, 1990.

[MAR 90] MARÉCHAL Y., "Modélisation des phénomènes magnétodynamiques avec terme de transport. Application aux ralentisseurs électromagnétiques, Thèse de Doctorat, Institut National Polytechnique de Grenoble, février 1991.

[MAU 88] MAUGIN G.A., "Continuum mechanics of electromagnetic solids", North-Holland, 1988.

[MAU 91] MAUGIN G.A.; "Compatibility of magnetic hysteresis with thermodynamics", *Int. J. of Appl. Electromag.* in Mat. 2, (1999), 7-19.

[OSS 99] OSSART F., HIRSINGER L., BILLARDON R., "Modelling of hysteresis losses in an electric machine stator subjected to assembling elastic stresses", 9th ISEM, *International Symposium on Nonlinear Electromagnetic Systems*, Pavia, may 10-12, 1999.

[ROU 96] ROUVE L.-L., OSSART F., WAECKERLÉ T., KEDOUS-LEBOUC A., "Magnetic flux and losses computation in electrical laminations", *IEEE Trans. Mag.*, Vol. 32, 5, (1996), 4219-4221.

[SAB 95] SABIR M., "Constitutive relations for magnetomechanical hysteresis in ferromagnetic materials", *Int. J. Engng. Sci.*, 33, 9 (1995) 1233-1249.